

Ignition condition and gain prediction for perturbed inertial confinement fusion targets

Roy KishonyDov Shvarts

Citation: [Physics of Plasmas](#) **8**, 4925 (2001); doi: 10.1063/1.1412009

View online: <http://dx.doi.org/10.1063/1.1412009>

View Table of Contents: <http://aip.scitation.org/toc/php/8/11>

Published by the [American Institute of Physics](#)

Articles you may be interested in

[Development of the indirect-drive approach to inertial confinement fusion and the target physics basis for ignition and gain](#)

[Physics of Plasmas](#) **2**, 3933 (1998); 10.1063/1.871025

[Hydrodynamic scaling of the deceleration-phase Rayleigh–Taylor instability](#)

[Physics of Plasmas](#) **22**, 072702 (2015); 10.1063/1.4923438

[Progress towards ignition on the National Ignition Facility](#)

[Physics of Plasmas](#) **20**, 070501 (2013); 10.1063/1.4816115



PFEIFFER VACUUM

VACUUM SOLUTIONS FROM A SINGLE SOURCE

Pfeiffer Vacuum stands for innovative and custom vacuum solutions worldwide, technological perfection, competent advice and reliable service.

Ignition condition and gain prediction for perturbed inertial confinement fusion targets

Roy Kishony

Physics Department, Nuclear Research Center-Negev, Beer-Sheva, Israel

Dov Shvarts^{a)}

*Physics Department, Nuclear Research Center-Negev, Beer-Sheva, Israel
and Mechanical Engineering and Physics Departments, Ben-Gurion University of the Negev,
Beer-Sheva, Israel*

(Received 19 April 2001; accepted 21 August 2001)

The effect of perturbations on hot spot ignition is studied using full two-dimensional (2D) numerical simulations of the National Ignition Facility [J. D. Lindl, *Phys. Plasmas* **2**, 3933 (1995)] direct drive Laboratory for Laser Energetics target design and newly derived 2D self-similar solutions for a perturbed burn wave propagation. It is shown that the required implosion velocity needed for ignition increases with the perturbation mode number and final amplitude, reaching an asymptotic value for high enough perturbation mode numbers, when the entire mixing zone no longer contributes to the ignition of the hot spot. Using the new self-similar solutions, ignition conditions for various perturbation mode numbers and amplitudes are obtained. These ignition conditions, which correspond to areal densities higher than needed for ignition in the symmetric case, are translated to a required increase in the implosion velocity needed for ignition, using the 1D Levendahl–Lindl scaling, in good agreement with the full 2D numerical simulation results. Finally, using the above results, a model for predicting the gain of a perturbed targets as a function of the perturbation spectra (single-mode and multi-mode) is presented, in good agreement with full numerical simulations. © 2001 American Institute of Physics. [DOI: 10.1063/1.1412009]

I. INTRODUCTION

The ignition of a central hot spot in the deuterium–tritium (DT) fuel, which generates a thermonuclear burn wave that propagates through the rest of the DT fuel, is crucial for achieving high gains in inertial confinement fusion.¹ Hot spot ignition and burn propagation are expected to be demonstrated in the National Ignition Facility (NIF).¹ The limited energy source of NIF is expected to provide relatively marginal hot spot ignition with relatively small areal densities.² The hot spot is thus sensitive to spatial perturbations which grow under the Rayleigh–Taylor instability and may quench the ignition. This motivates a detailed investigation of the conditions under which the hot spot ignites and of the effects of spatial perturbations on these conditions.²

The ignition conditions are often determined using simplified, zero-dimensional (0D), Widner-type models of the hot spot.^{3–9} These models describe the hot spot by few characteristic variables: The radius R , density ρ , and temperature T . The ignition line (IL) is then defined as the line in the ρR – T plane on which the energy loss and gain rates inside the hot spot are balanced. In a previous work,¹⁰ we showed that a set of self-similar solutions, the existence of which was first pointed out by Neudachin and Sasorov,^{11,12} can be used to provide the ignition criteria while accounting for the radial critical profiles of the hydrodynamic variables inside the hot spot. The self-similar solutions exist for an outside density profile ρ_{out} that decreases as $1/r$ and it includes all the rel-

evant physical mechanisms. It was shown that although this special boundary condition under which the self-similar solutions exist, they provide a natural global ignition condition that is applicable for more general density profiles.

The main uncertainty in the design of ignition facilities, such as NIF, results from the effect of perturbations.¹ The literature presents several numerical investigations of the effect of perturbations on target ignition and gain. Effects of single mode long wavelength perturbations were studied by the Rochester group (Verdon¹³ and McCrory and Verdon¹⁴) and later by Atzeni.^{15–17} Perturbations with different mode numbers l and different amplitudes A were investigated by means of a two-dimensional (2D) numerical simulation. It was found that the yield of the target decreases as the initial perturbation amplitude A increases or as the mode number l increases. For a given mode number l there exists a critical initial amplitude above which ignition does not occur. The critical initial amplitude was found to decrease with the mode number l of the perturbation.

Haan *et al.*² estimated the robustness of the NIF baseline target design to hydrodynamic instabilities, which result from the surface roughness. They used direct single mode 2D calculations at different modes, combined with a saturation model,¹⁸ to estimate the perturbation amplitude at peak compression that results from a given surface roughness. The effect of the perturbation on ignition was modeled by direct 2D simulations. It was found that spike amplitude of 30%–50% of the hot spot radius would quench the ignition.

Direct 2D and 3D simulations of the NIF target with

^{a)}Electronic mail: schwartz@bgumail.bgu.ac.il

multimode perturbations were only recently studied.^{19–22} The perturbed hot spot is seen to consist of a central clean region of low density D–T, surrounded by a mixing zone, composed of wide bubbles of the low density D–T floating outside through the high density spikes. Although the initial perturbation contains many modes, the final perturbation is usually characterized by a single dominant wavelength, motivating the single mode approach taken in the current work.

Levedahl and Lindl²³ analyzed the effect of a short wavelength mixing zone surrounding the hot spot on ignition. They derived a scaling law for the increase in the implosion velocity required for ignition as a function of the thickness of the mixing zone.

In the current work the effect of perturbations on hot spot ignition is studied using full two-dimensional simulations and new two-dimensional self-similar solutions. The simulations' results are presented and discussed in Sec. II. In Sec. III we compare the results with Levedahl and Lindl's²³ formula. It is shown that their formula describe well the results of high mode number perturbations, but is not adequate for describing low modes. Section IV presents a model for the effect of perturbation on hot spot ignition, which is adequate for a wide region of mode numbers. The model is based on new 2D self-similar solutions derived as an extension, proposed by Neudachin and Sasorov,^{11,12} to the 1D self-similar solutions presented in Ref. 10. Using these 2D self-similar solutions, an ignition condition for perturbed hot spots is obtained as a function of the perturbation mode number and final amplitude. We then combine the 2D self-similar ignition condition with Levedahl and Lindl's²³ scaling law to give the increase in the implosion velocity required for ignition. Finally, in Sec. IV, we give an approximate formula for the yield of a general perturbed target as a function of the implosion velocity and the perturbation spectrum both for single mode and for multimode perturbations.

II. TWO-DIMENSIONAL NUMERICAL SIMULATIONS FOR PERTURBED HOT SPOTS

Since real hot spots, as was discussed in the Introduction, are usually dominated by a single mode at the time of ignition, we concentrate on single mode perturbations. We repeat the single mode calculations found in the literature^{13–17} and extend them to higher mode numbers. For high l 's a new behavior is obtained—the initial critical amplitude A_C no longer decreases with l , but starts to increase. This new behavior is presented and discussed.

A. Description of the 2D simulations geometry and the simulation code

Three-dimensional calculations indicate that the multi-mode 3D perturbation is an array of spikes penetrating the hot spot, surrounding approximately hexagonal bubbles.^{2,20} These 3D perturbations can be simulated directly using 3D numerical codes,^{24–26} or can be approximated by 2D codes in various geometries. Both the Rochester group^{13,14} and Atzeni^{15–17} chose a 2D representation of the perturbations by spherical harmonic modes with $m=0$ (Legendre polynomial modes). Following Haan,² we chose the approach of a 2D

Cone approximation, described below, which is more adequate for modeling the 3D structures of bubbles and spikes that are present in reality. Moreover, the Cone approach allows the computation of relatively high mode numbers with a still reasonable numerical resolution.

For a given wavelength, two different 3D configurations exist.^{20,26} The first configuration describes bubbles that are surrounded by spikes (bubble-ridge configuration) and the second configuration describes spikes surrounded by bubbles (valley-spike configuration). Haan proposed that these two 3D configurations could be approximated in 2D simulations within a Cone with reflective boundary conditions.² The first configuration is approximated by a single bubble of appropriate solid angle surrounded by a spike curtain falling along the reflective boundary conditions of the Cone.² The second configuration is of opposite sign—a spike on the axis of the Cone surrounded by a circular bubble.²

In the present work we adopt the Cone approximation approach and focus mainly on the spike-on-axis configuration, which has greater effect on ignition. A comparison between spike-on-axis and bubble-on-axis configurations is brought in Sec. IV.

The simulations were performed on profiles close²⁷ to C . Verdon's canonical direct drive design of NIF.^{28–30} A velocity perturbation with a given mode number l and amplitude A was imposed on the 1D profiles of this target, before the time the Rayleigh–Taylor instability begins (the 1D profiles were taken from Ref. 31)

$$v_{2D}(r, \theta) = v_{1D}(r)(1 + A \cos(l\theta)).$$

The simulations were performed in a Cone with an angle of $2\pi/l$ and with reflective boundary conditions. We shall refer to l as the mode number of the perturbation, although it does not correspond to a pure Legendre polynomial mode. The initial perturbation amplitude is denoted by A to distinguish it from the final perturbation amplitude ξ of the hot spot at the time of stagnation.

The simulation code used is the LEEOR-2D code.^{32,33} The code includes hydrodynamics, electron heat conduction, fusion, a simple one group diffusion model for α -particle transport and bremsstrahlung radiation losses. An ideal gas equation of state was used for the DT fuel.

The code assumes equal ion and electron temperatures because of their relatively small relaxation time. Fuel depletion is not taken into account, as it is relatively low in NIF targets due to the low ρR of the shell and, in general, its main effect is during the burn stage and it barely affects the ignition stage in which we are interested. Taking into account all these mechanisms, the resulting gain of the target was found to be very close to the gain calculated by Verdon^{29,30} for the same target.²⁷

For the calculations presented here we used a $r-\theta$ geometry mesh. Typically, the mesh consists of 15 cells in the θ direction (15 cells per half wavelength) and 65 cells in the r direction. The rezoning scheme was set to keep an equal partitioning in the θ axis. In the radial direction the scheme was set to move the cells of the hot spot shell lagrangianly while keeping the inner hot spot cells uniformly distributed between the center of the hot spot and the moving shell.

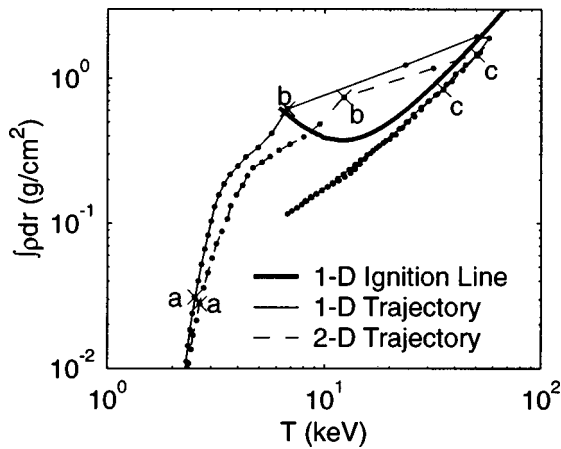


FIG. 1. The $\rho R - T$ plane (with $\rho R = \int \rho dr$). Shown are the self-similar ignition line for a symmetric hot spot and trajectories of a symmetric hot spot and of a perturbed hot spot with mode number $l=6$ and initial amplitude $A=2.5\%$. The dots indicate Δt of 25 ps. The times of implosion, ignition, and burn wave propagation are marked by a, b and c, respectively.

B. The time evolution of a perturbed capsule

As a typical example of a simulation of a perturbed hot spot, we choose the case of mode number $l=6$ and initial velocity amplitude $A=2.5\%$, for which the resulting final amplitude $\xi = \Delta R/R$ is 22%. This perturbation is not large enough to quench the ignition and the development of the hot spot both before and after ignition can thus be followed and compared with the development of the unperturbed hot spot. Figure 1 compares the trajectories in the $\rho R - T$ plane of the perturbed and unperturbed targets.

In the early implosion stage the hot spot is still Rayleigh–Taylor stable, the perturbation is small and the trajectories are relatively close. Then, at about the time marked by “a” in Fig. 1, the Rayleigh–Taylor instability begins, the perturbation starts to grow and the trajectories diverge from each other.

The time of ignition, marked by “b” in Fig. 1, is characterized by a sudden increase in the hot spot temperature. This sudden increase is seen by the distance between the points along the trajectories, which are marked at time intervals of 25 ps. It is seen that the ignition of the symmetric case occurs as the 1D self-similar IL¹⁰ is crossed. Ignition of the perturbed hot spot, however, is seen to occur above the IL. The hot spot at that time is highly perturbed ($\Delta R/R = 0.22$), which increases the energy loss rates from the hot spot and thus requires a higher ρR for ignition. In other words, the IL’s for perturbed hot spot should be higher than the IL derived for the symmetric hot spot. After ignition the trajectories propagate along a working line which is parallel to the stable right branch of the IL. At this stage, the propagation of the burn smears out the perturbation and thus the perturbed hot spot propagates along the same working line as the symmetric hot spot.¹⁰

C. The critical initial and final amplitudes

The resulting yields and critical amplitudes of the various simulations performed are summarized in Fig. 2(a). The

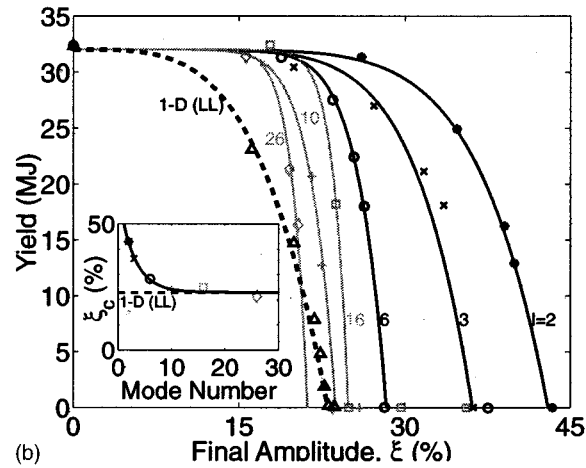
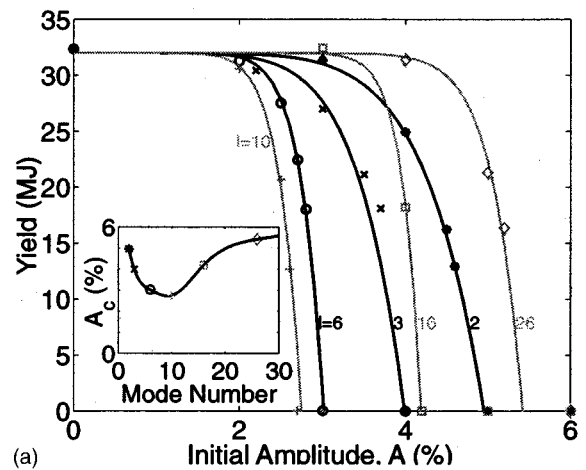


FIG. 2. Yield of perturbed hot spots versus the perturbation initial (a) and final (b) amplitude for different mode numbers between 2 and 26. Inset: the critical amplitude versus the perturbation mode number. Figure (b) also shows the yield of the symmetric 1D case in which the implosion velocity is reduced by Δv as a function of the effective perturbation associated with that reduction [Eq. (2)].

figure shows the yield of the target relative to the yield of the unperturbed target as a function of the initial perturbation amplitude for different mode numbers. This figure is analogous to the figures shown in Refs. 13–17, except that it is extended to higher mode numbers. The critical initial amplitude is shown in the inset as a function of the perturbation mode number.

Our calculations indicate a new behavior in the extension of the results of Refs. 13–17 to high mode numbers. It is seen from Fig. 2(a) that at high l ’s, the critical amplitude A_c no longer decreases with l , but starts to increase. Thus, the moderate wave numbers (of $l=5-12$) are the most dangerous ones. The different behavior seen in low and high mode number is, as explained below, due to the effects of two different physics: The Rayleigh–Taylor growth of the modes is the dominant physics that determines the critical amplitude in high mode numbers and the effect of a given mode on ignition is the dominant physics in low mode numbers.

The effect of the different Rayleigh–Taylor growth factors of the different modes is eliminated in Fig. 2(b), which shows the same data of Fig. 2(a), but as a function of the

final amplitude of the hot spot defined by $\xi = \Delta R/R_0$ at the time of peak compression. This way, only the ignition physics is left; decreasing the mode number causes a decrease in the effective area to volume ratio, which allows ignition with higher amplitudes.

Hence, the increase in the critical initial amplitude with the mode number seen in Fig. 2(a) in the high mode region is not a result of a reduced effect of the higher mode on ignition, but is a consequence of the reduced Rayleigh–Taylor growth factors of the high modes. An increase in the mode number in this region causes a decrease in the growth factor due to early saturation of the higher modes.

It is seen in Fig. 2(b) that as l becomes higher than some specific wave number l^* (which is approximately 8 in our case) the critical final amplitude ξ_C does not increase with increasing l , but converges asymptotically to a certain value. This asymptotic behavior results from the fact that in the region of mode numbers higher than l^* the bubbles do not contribute any more to the fusion process and they no longer help in the ignition process. In this region only the clean inner part of the hot spot contributes to ignition and thus the critical final amplitude no longer depends on the perturbation mode number. The fact that for high mode numbers only the clean inner part of the hot spot contributes to ignition was used by Levedahl and Lindl²³ to determine the required increase in the implosion velocity needed to ignite hot spots with high mode number perturbations, as described in the next section.

III. THE IMPLOSION VELOCITY REQUIRED FOR IGNITION OF A PERTURBED HOT SPOT

From the practical point of view, the most important result of studying the effect of perturbations is to specify the required increase in the implosion velocity needed for ignition in the presence of a perturbation. For high mode number perturbations, Levedahl and Lindl²³ suggested a simple, but yet powerful, scaling law that relates the required increase in the implosion velocity to the amplitude of the perturbations. Levedahl and Lindl's idea consists of two main assumptions. The first is that for perturbations with high mode numbers [see Fig. 5(a) below], only the inner clean part of the hot spot contributes to ignition. The second is that the required increase in the velocity is of the same magnitude that would have been required if the entire capsule had been rescaled in size by the ratio, R_{clean}/R_0 , of the clean to unperturbed hot spot radii. Then, using Livermore scaling law $E_{\text{ign}} \propto v^{-5.5}$ between the driver energy required for ignition and the achieved target implosion velocity,¹ the relation between the required increase in the implosion velocity and the perturbation amplitude was obtained²³

$$\frac{v_{\text{mix}}}{v_0} = \left(\frac{R_{\text{clean}}(\xi)}{R_0} \right)^{-2/5} = (1 - \xi)^{-2/5}. \quad (1)$$

The resulting increase, v_{mix}/v_0 , in the implosion velocity required for ignition when high mode number perturbations are present is shown below in Fig. 9(b). Note that Livermore scaling law apply to the class of implosions in which the implosion pressure is kept constant while the implosion ve-

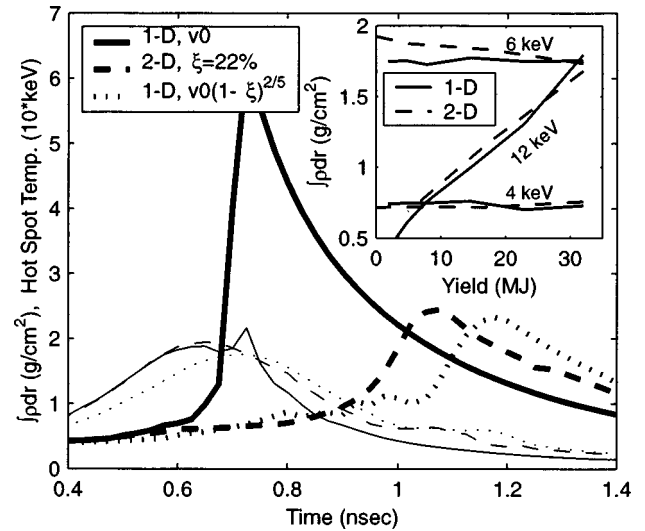


FIG. 3. The total optical depth of the target (thin lines) and the hot spot temperature (thick lines) are shown as a function of time for three targets: an unperturbed target with implosion velocity v_0 (1D), a perturbed target with $l=10$, $\xi=22\%$, and v_0 (2D), and a symmetric target with reduced implosion velocity $v=v_0(1-\xi)^{2/5}$ (1D*). Inset: The total optical depth at the moments in which the hot spot temperature reaches 4, 6, and 12 keV versus the target yield as the perturbation amplitude ξ is varied (2D) and as the corresponding implosion velocity in a symmetric target is varied (1D*).

locity or fuel entropy is changed. Other classes of implosions result different scaling laws^{34–36} and are not considered in the current work.

Let us now phrase the relation of Eq. (1) from a somewhat different point of view. Since a perturbation can be compensated by an increase in the implosion velocity, we may say that the perturbation is equivalent to a decrease in the implosion velocity by the same amount. A symmetric hot spot with implosion velocity reduced by Δv would thus be the equivalent of a perturbed hot spot with an amplitude ξ defined by

$$\xi = 1 - [(v_0 - \Delta v)/v_0]^{5/2}. \quad (2)$$

In Fig. 2(b) this formula was used to plot the yield of 1D simulations of a symmetric hot spot in which the nominal implosion velocity v_0 was reduced by a varied amount, Δv . As expected, it is seen [Fig. 2(b) inset] that Levedahl and Lindl's 1D model represents the asymptote at large l 's of the ignition threshold of full 2D simulations. Less expected, however, is the fact that the model describes well not only the ignition threshold but also the whole gain curve of high mode number targets. In general, the burn efficiency of a target depends only on its total $\int \rho dr$ once it has ignited. Levedahl and Lindl's model, however, describes the effect of mix on the implosion velocity required to achieve ignition and says nothing about burn efficiency or yield. To understand how could the ignition model of Levedahl and Lindl's be extended to gain prediction,³⁷ we refer to Fig. 3. The figure shows, as a function of time, the average temperature of the hot spot and the total target optical depth ($\int \rho dr$) for three variations of the target: An unperturbed target with implosion velocity v_0 (1D), a perturbed target with $l=10$, $\xi=22\%$ and the same implosion velocity v_0 (2D), and a sym-

metric target with reduced implosion velocity $v = v_0(1 - \xi)^{2/5}$ ($1D^*$). The $1D$ target has a yield of 32 MJ and both the $2D$ target and the $1D^*$ target have a yield of about 5 MJ, which is a demanding point right on the gain cliff. As seen in the figure, the cause for the reduction in yield is not a result of a reduction in the maximal optical depth achieved, which is hardly affected by neither the $2D$ perturbation nor by the $1D^*$ reduced velocity (the reduced velocity naturally causes a slight delay in the implosion schedule, but the maximal optical depth is barely affected). Looking at the hot spot temperature, however, it is seen that unlike the $1D$ target which ignites in concert with the maximal optical depth, the $2D$ and the $1D^*$ targets ignite much later when the target optical depth is considerably lower. This lower optical depth at the time of ignition is responsible for the reduced yield of the target. This is also seen in the figure inset which summarizes the results of targets with other perturbation amplitudes ξ and their corresponding symmetric targets with reduced velocity. The inset shows the relation between the total yield of the target and its optical depth taken at times when the hot spot temperature reaches 4, 6, and 12 keV. Looking at the optical depth at the time when the hot spot temperature reaches 12 keV, it is seen that the yield is a function of the optical depth alone and scales in the same way for the $2D$ and for the $1D$ cases. It is also seen that at slightly earlier times, when the hot spot temperature is 4–6 keV, the optical depth of both the $1D$ and the $2D$ cases is totally independent of the target's yield. The $2D$ perturbation and the reduced velocity in the $1D$ case thus seem to affect the yield by disturbing and delaying the ignition process allowing more time for the target to expand and thus reducing the actual optical depth of the target at the time of ignition. Levedahl and Lindl's model indeed describes only the effect of perturbation on *ignition*, but it does it so well that not only it gives the threshold for ignition, but also the right delay in ignition for marginal targets. This right delay in ignition is then translated to the right reduction in the optical depth and thus to the right yield for the target.

It is apparent, however, from Fig. 2(b) that the Levedahl and Lindl's formula does not explain the relatively high final amplitudes needed to quench the ignition for low mode number perturbations. In order to explain the difference between low and high perturbation mode numbers, let us now compare these two limits. Figure 4 compares the temperature contours and radial profiles at the time of ignition, when the temperature at the center of the hot spot is 13 keV, for two different simulations with mode numbers 3 and 16 and with initial amplitudes chosen as to achieve marginal ignition defined by the same gain ($G=2$). Although the temperature at the center of the hot spot is the same, the temperature of the hot spot's bubbles is much higher in the low mode case than in the high mode case. This is seen both from the relative proximity of the 1.5 and 7 keV contours in Fig. 4(a) and from the temperature along the "bubble" profiles in Fig. 4(b). This difference in the bubble temperature between low modes and high modes, which is due to the high tangential energy losses in the high mode bubbles, allows the low mode hot spot to ignite with higher perturbation amplitudes at peak compression (in the example shown, the $l=3$ hot spot ignites

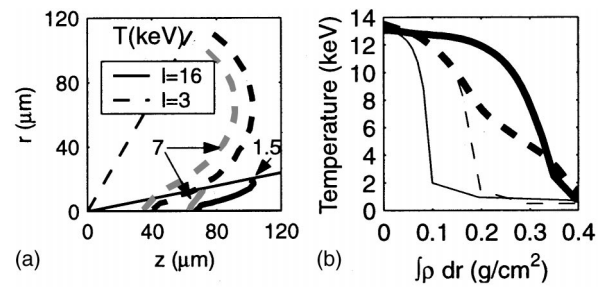


FIG. 4. Comparison between low mode ($l=3$) and high mode ($l=16$) perturbations with different initial amplitudes chosen to get the same gain ($G=2$). Shown at the time of ignition are the temperature contours (a) and the temperature profiles as a function of $\int \rho dr$ along the Cone surface (thick lines), where the bubbles are located, and along its axis (thin lines), where the spikes are located (b).

with an amplitude of about 33% in peak compression relative to only 22% for the $l=16$ case). Indeed, it is seen that while the tips of the bubbles of the two hot spots reach approximately the same radius [about $110 \mu\text{m}$ in Fig. 4(a)] and the same optical depth [about 0.4 g/cm^2 in Fig. 4(b)], the spike of the $l=3$ hot spot penetrates much more than in the $l=16$ case ($0.1 \text{ g/cm}^2, 40 \mu\text{m}$ versus $0.2 \text{ g/cm}^2, 70 \mu\text{m}$) and still both targets ignite in the same way and achieve the same total yield.

The Levedahl and Lindl argument can be formally extended to include also the effect of perturbations with low mode numbers. As we have seen, for low mode numbers the bubbles still contribute to the ignition of the hot spot. Hence, the perturbed hot spot should be equivalent to an unperturbed symmetric hot spot with an effective radius, R_{eff} , that is lower than the unperturbed radius R_0 , but higher than the inner clean radius R_{clean} [see Fig. 5(b)]. Given the effective radius, $R_{\text{eff}}(l, \xi)$, as a function of the perturbation's mode number and amplitude the increase in the velocity required for ignition is given using the same formula that Levedahl and Lindl used, except that now $R_{\text{clean}}(\xi)$ should be replaced with $R_{\text{eff}}(l, \xi)$

$$\frac{v_{\text{mix}}}{v_0} = \left(\frac{R_{\text{eff}}(l, \xi)}{R_0} \right)^{-2/5} = \hat{R}_{\text{eff}}(l, \xi)^{-2/5}. \quad (3)$$

The main difficulty in using Eq. (3) for determining the required increase in the implosion velocity is to obtain the

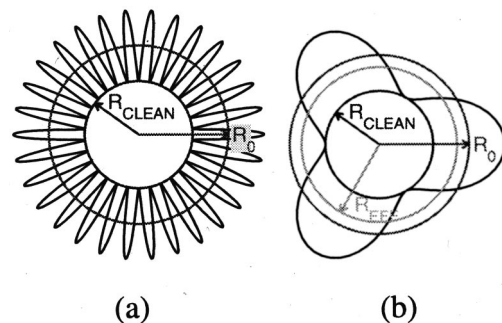


FIG. 5. Schematic illustration of a hot spot with a high (a) and low (b) mode number perturbation.

normalized effective radius $\hat{R}_{\text{eff}}(l, \xi)$ and its dependence on the perturbation mode number and amplitude.

For high mode numbers the Levedahl and Lindl formula should be reproduced and we thus expect $\hat{R}_{\text{eff}}(l, \xi) \xrightarrow{l \rightarrow \infty} 1 - \xi$, which means that only the clean inner part of the hot spot contributes to ignition. For low mode numbers the bubble still contributes to ignition and we should expect $\hat{R}_{\text{eff}}(l, \xi)$ to be somewhere between the spike tips, $1 - \xi$, and the bubble tips, $1 + \xi$. In the next section we shall see that new 2D self-similar solutions can be used to obtain the effective radius.

IV. IGNITION CRITERIA USING TWO-DIMENSIONAL SELF-SIMILAR SOLUTIONS

As was shown in Sec. II, the hot spot's thermodynamic properties are hardly affected by perturbations in the implosion stage and their main influence is during the approach to ignition stage. In this section the ignition conditions for perturbed hot spots are derived using new 2D self-similar solutions. The derived ignition criteria will then be used to define the required increase in the implosion velocity needed for ignition and the yield of a perturbed target.

A. The two-dimensional self-similar solutions

In Ref. 10 it was shown that self-similar solutions for the propagation of the hot spot, which include all the relevant physical mechanisms, exist for an outside density profile $\rho_{\text{out}} = s/r$. The set of 1D self-similar solutions with different values of the parameter s was mapped into the $\rho R - T$ plane to obtain the IL for symmetric hot spots. We shall now see that the same procedure can be applied for perturbed hot spots, namely deriving 2D self-similar solutions and use these solutions to obtain the ignition criteria for perturbed hot spots.³⁸

The 1D self-similar solutions can be extended to include spatial perturbations by imposing a modulation on the outside density profile of the form

$$\rho_{\text{out}}(r, \theta) = \frac{s}{r} (1 + \epsilon \cos \theta l). \quad (4)$$

This way, no new dimensional parameters are introduced and the solution should, therefore, remain self-similar.

In the 1D case, the separation of variables reduced the partial differential equations to ordinary differential equations in the variable $\zeta = r/R(t)$. These equations could be solved by a simple numerical integration. In the 2D case, however, the equations cannot be reduced to ordinary differential equations. After reducing the time variable from the 2D equations, a set of partial differential equations with two variables ζ and θ is obtained. Hence, the 2D self-similar solutions could not be obtained by means of a simple numerical integration. Instead, we obtained the solutions using 2D simulation in which an initial hot spot is ignited at the center of a density profile of the form of Eq. (4). The solution was found to converge to the asymptotic self-similar solution after the burn wave propagates a few initial hot spot radii.

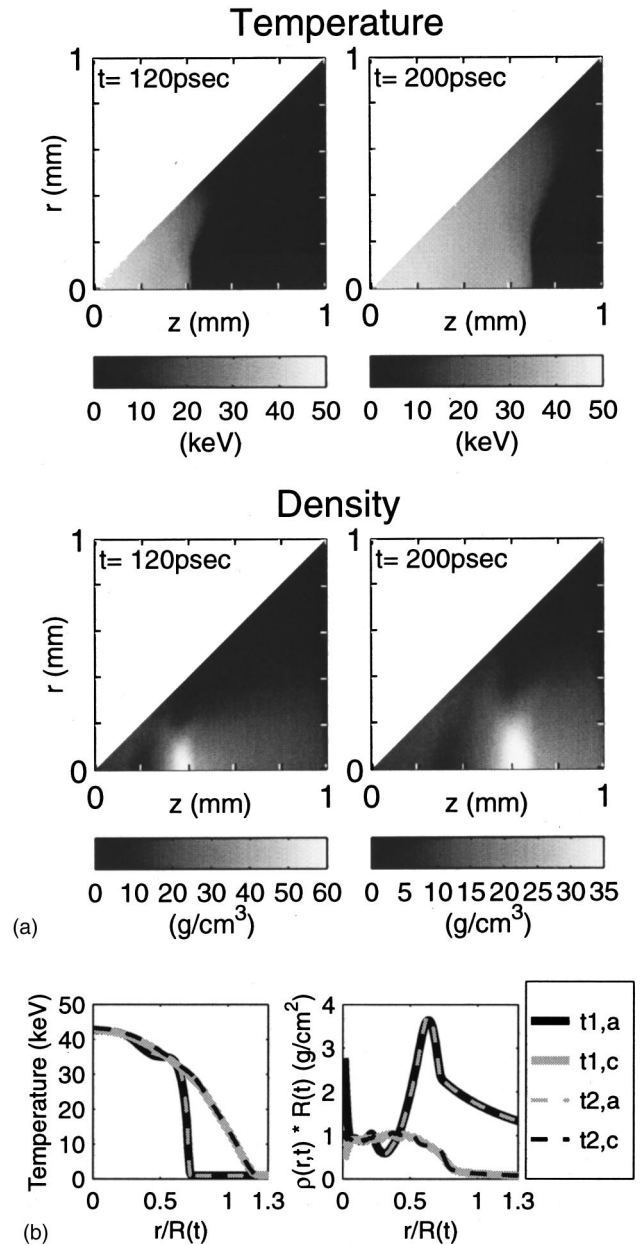


FIG. 6. A typical 2D self-similar solution at two different times. (a) Temperature and density contours. (b) Radial profiles of the temperature and density (multiplied by the hot spot radius) along the Cone axis ($t1,a$ and $t2,a$) and along the Cone surface ($t1,c$ and $t2,c$).

This approach is analogous to Neudachin and Sasorov's approach for the 1D solutions^{11,12} and it allows only the stable solutions to be obtained.

An example of a 2D self-similar solution for a perturbed hot spot with $\rho R = 0.6 \text{ g/cm}^2$,³⁹ $l = 6$ and $\epsilon = 0.9$ is given in Fig. 6. Figure 6(a) shows the temperature and density contours of the hot spot and the surrounding cold fuel at two different times. Figure 6(b) shows the radial profiles of the temperature and density on the Cone surface (bubble) and along the Cone axis (spike). It is seen that the whole 2D maps of the temperature and the density are similar to themselves up to changes of scale. As in the 1D case, the scale of the temperature does not change with time, while the density scale decreases as $1/t$ (or $1/R$, since $R \propto t$). To emphasize

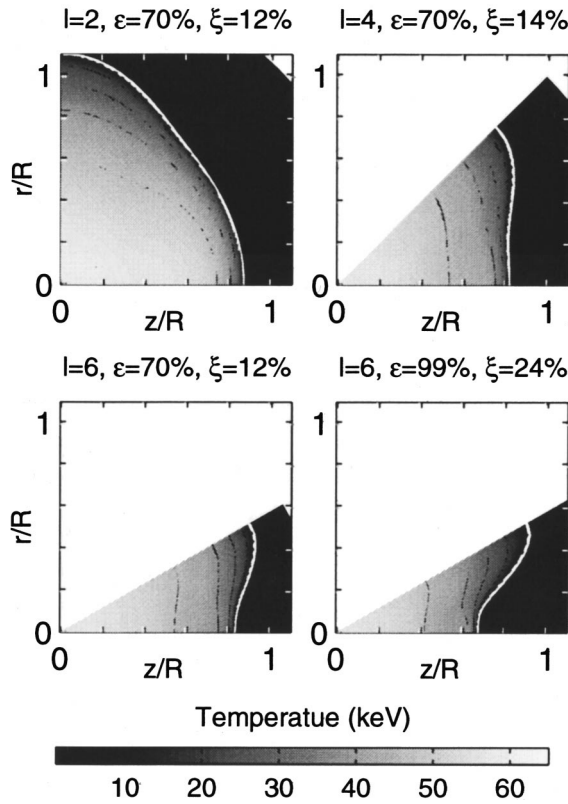


FIG. 7. Temperature contours of spike-on-axis 2D self-similar solutions for different perturbation mode numbers and amplitudes.

these scalings, the density profiles in Fig. 6(b) were multiplied by the hot spot radius and the color scales in Fig. 6(a) were drawn according to the scaling of the corresponding variables (the temperature scale is 0–50 keV for both values of t , while the density scale is 0–60 g/cm³ for $t = 120$ ps and 0–35 g/cm³ for $t = 200$ ps according to the $1/t$ dependence).

The solution shown in Fig. 6 is only an example; there is actually a three parameter family of self-similar solutions determined by the boundary condition parameters: The optical depth parameter s , the perturbation mode number l and the perturbation amplitude ϵ .

The solutions with $\epsilon > 0$ describe spike-on-axis perturbations (see the temperature contours in Fig. 6) and those with $\epsilon < 0$ describe bubble-on-axis perturbations. We shall now present the spike-on-axis solutions in more details. For bubble-on-axis perturbation, concluding results are shown and a comparison with the spike-on-axis solutions is made. In general the bubble-on-axis results are similar to the spike-on-axis results except for the case of $l = 2$, which will be considered separately. Figure 7 shows the temperature profiles of four self-similar solutions with the same effective ρR and different amplitudes, ϵ , and mode numbers, l , of the outside density modulation. For each 2D self-similar solution, the perturbation amplitude $\xi = \Delta R/R$,⁴⁰ which is a time independent parameter characterizing each solution, is indicated in the figure. The amplitude ξ is a monotonic function of the amplitude ϵ . However, even when ϵ approaches 100%, the obtained amplitude ξ of the resulting hot spots is bounded ($\xi = 24\%$ for $\epsilon = 99\%$ and $l = 6$ in the case shown in

Fig. 7). The physical cause of this limit of ξ is the tangential energy transport mechanisms, which tend to heat and reduce the cold spikes penetrating the hot spot. We should expect these tangential conduction mechanisms to decrease as the wavelength of the perturbation is increased and thus larger perturbation amplitudes ξ should be obtained for smaller perturbation mode numbers. This can be seen when comparing $l = 4$ and $l = 6$ with $\epsilon = 70\%$, which result $\xi = 14\%$ and 12% , respectively.

For small modulation amplitudes the 2D self-similar solution is similar to its corresponding 1D self-similar solution. However, the interesting solutions, from the point of view of the ignition conditions, are those with relatively high perturbation amplitudes. In these solutions the tangential mechanisms become important for the ignition process (see also Fig. 4) and the propagation of the thermonuclear burn wave is possible due to these tangential mechanisms. Without tangential interaction, the 2D solution would be composed of a series of 1D solutions, such that the profiles along any direction, θ , are the profiles of the 1D self-similar solution that corresponds to the boundary condition parameter $s_{1D} = s(1 + \epsilon \cos \theta)$. For the high modulation amplitudes shown in Fig. 7 and for θ close to the Cone surface, s_{1D} is actually lower than the critical value s_{cr} , defined in Ref. 10 as the value of s below which there are no 1D self-similar solutions. The propagation of a thermonuclear burn wave along these θ 's is thus possible only due to the tangential mechanisms.

B. Ignition criteria for perturbed hot spots using the 2D self-similar solution

For each mode number, l , and hot spot amplitude, ξ , a set of 2D self-similar solutions exist for different values of the parameter s .⁴¹ Each of these sets can be mapped into the $\rho R - T$ plane to produce the IL for a hot spot with the given perturbation mode number and amplitude. The mapping is done using the following definitions:

$$\bar{T} = \frac{1}{M} \int_V \rho T dV,$$

$$\rho R = \frac{1}{1 - \cos(\pi/l)} \int_0^{\pi/l} \frac{3}{2} s(1 + \epsilon \cos l\theta) \sin \theta d\theta, \quad (5)$$

which are the natural extensions of the definitions used for the symmetric case, in Ref. 10.

The resulting IL's are shown in Fig. 8 together with the IL of the unperturbed hot spot. It is seen that the IL's of the perturbed hot spots are higher than the IL of the symmetric hot spot (except for the $l = 2$ case with relatively low amplitudes, which will be discussed below). The lines get higher as the perturbation amplitude is increased and as the mode number is increased. A higher IL means that larger hot spots, with higher ρR , must be produced in order to achieve ignition in the presence of perturbations. This is in agreement with the results of the simulations presented in Fig. 1, where it was shown that perturbed hot spots ignite at higher ρR than the unperturbed hot spot. A complete comparison with the simulation results is brought in the next subsection.

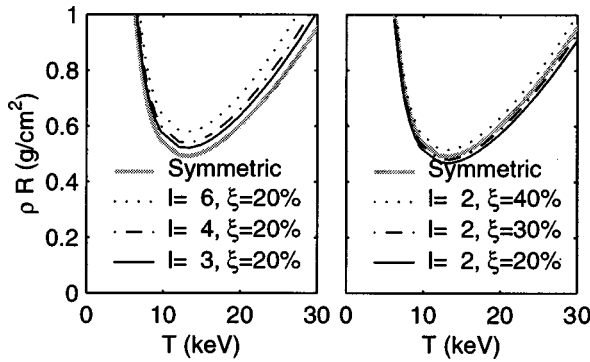


FIG. 8. The ignition lines in the $\rho R - T$ plane for perturbed spike-on-axis hot spots compared to the ignition line for symmetric hot spot. The ignition lines for the perturbed cases were obtained only for the stable right branch and were extrapolated to the unstable left branch keeping a constant distance from the 1D ignition line.

C. The required increase in the implosion velocity needed for ignition

The higher ρR needed to ignite a perturbed hot spot can be related to a higher implosion velocity needed for ignition. In Eq. (3), the increase in the required implosion velocity was defined in terms of the effective radius of the hot spot. The idea is that the effective radius as a function of the perturbation's mode number and amplitude can be reduced from the 2D self-similar IL's presented in Fig. 8. Using these IL's, the ratio of the effective to the unperturbed radius is defined by

$$\frac{R_{\text{eff}}(l, \xi)}{R_0} = \frac{(\rho R)_{\text{min}}^{\text{1D}}}{(\rho R)_{\text{min}}^{l, \xi}}$$

where $(\rho R)_{\text{min}}^{\text{1D}}$ is defined as the minimal ρR along the 1D self-similar IL and $(\rho R)_{\text{min}}^{l, \xi}$ is defined as the minimal ρR along the 2D self-similar IL of a perturbed hot spot with the given perturbation mode number l and amplitude ξ . The obtained effective radius is shown in Fig. 9(a). It is seen that, except for the $l=2$ case, the effective radius is lower than the unperturbed radius and it decreases with the perturbation amplitude and with the perturbation mode number. As expected, the effective radius is always higher than the clean radius of the spike tips and converges to it as $l \rightarrow \infty$.

The effective radius of the self-similar solutions was introduced into Eq. (3) to obtain the required increase in the implosion velocity needed for ignition. The resulting implosion velocity is shown in Fig. 9(b) as a function of the perturbation amplitude at peak compression for different mode numbers. The $l=\infty$ line corresponds to the results of Levedahl and Lindl. It is seen that the lines of the high mode numbers ($l=6$ and 12) are relatively close to the $l=\infty$ line and coverage to it as the perturbation amplitude is increased. This convergence is seen to occur for $\xi \gg 1/l$ as the aspect ratio of the bubbles becomes high enough so that the bubbles no longer contribute to ignition. For low mode numbers (the $l < 4$ lines) the bubbles do contribute to ignition and the required velocity is thus lower than the results of Levedahl and Lindl. For the mode numbers $l > 2$, it is seen in Fig. 9 that the bubble-on-axis ($\epsilon < 0$) results are similar in nature to the

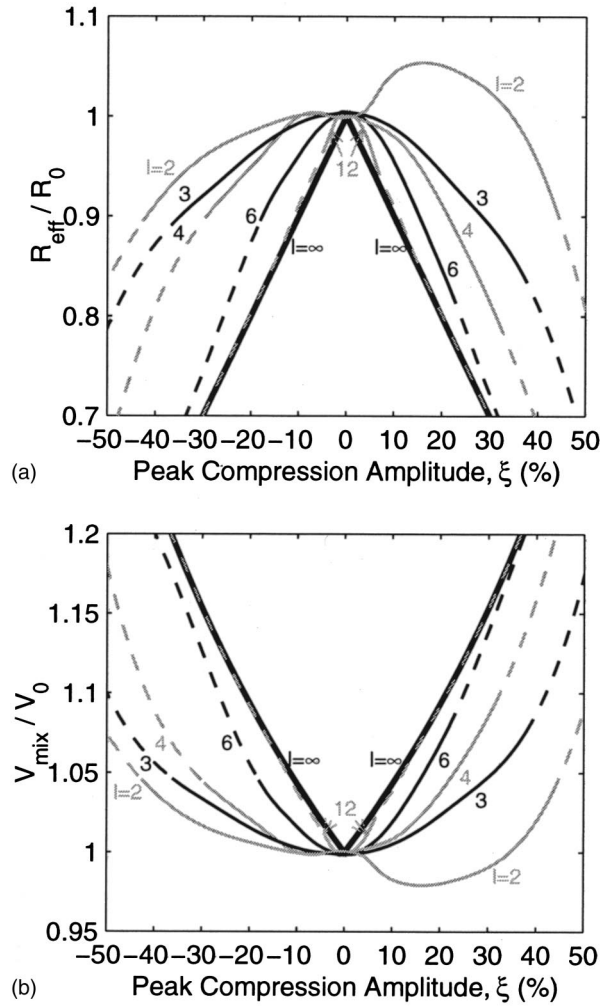


FIG. 9. The normalized effective radius (a) and the corresponding increase in the implosion velocity required for ignition (b) versus the perturbation amplitude at peak compression for different perturbation mode numbers. Positive amplitudes correspond to spike-on-axis and negative amplitudes correspond to bubble-on-axis, except for $l=2$ where the situation is opposite. The lines were extrapolated (dashed lines) to the region of high perturbation amplitudes for which the self-similar solutions do not exist.

spike-on-axis ($\epsilon > 0$) results. For the bubble-on-axis configuration, a slightly lower implosion velocity is needed than for the spike-on-axis configuration.

For the mode number $l=2$, an apparent anomalous behavior is obtained. According to the self-similar solutions, up to amplitudes of about 30% the required implosion velocity needed for ignition is *smaller* than that needed for the symmetric case. In other words, an $l=2$ perturbation with a low amplitude may actually help the ignition of the hot spot.

This apparent anomalous behavior, predicted by the 2D self-similar solutions, is verified in Fig. 10 by means of direct 2D simulations. The figure shows the yield of a target with an implosion velocity slightly above the critical velocity needed for ignition, versus the perturbation amplitude at peak compression for amplitudes with mode number $l=2$. Indeed, in agreement with the prediction of the self-similar solutions, small perturbation amplitudes are seen to increase the yield of the target. However, at first sight, it seems that

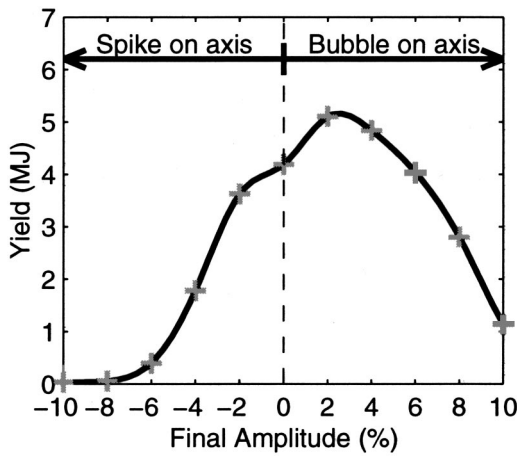


FIG. 10. Target yield versus perturbation amplitude for $l=2$. An increase in the yield is seen for small bubble-on-axis perturbations.

there is a discrepancy in the sign of the perturbation amplitude; in the simulations the yield is increased for bubble-on-axis perturbations, while the self-similar solutions were obtained for spike-on-axis perturbations.

This discrepancy is a result of a phase reversal in the self-similar solutions of $l=2$ as demonstrated in Fig. 11. The figure shows the temperature contours of self-similar solutions with $l=2$ and 6 for negative and positive perturbation amplitudes, ϵ . It is seen that while the contour of 4 keV, according to which the amplitude ξ was defined, is in a spike

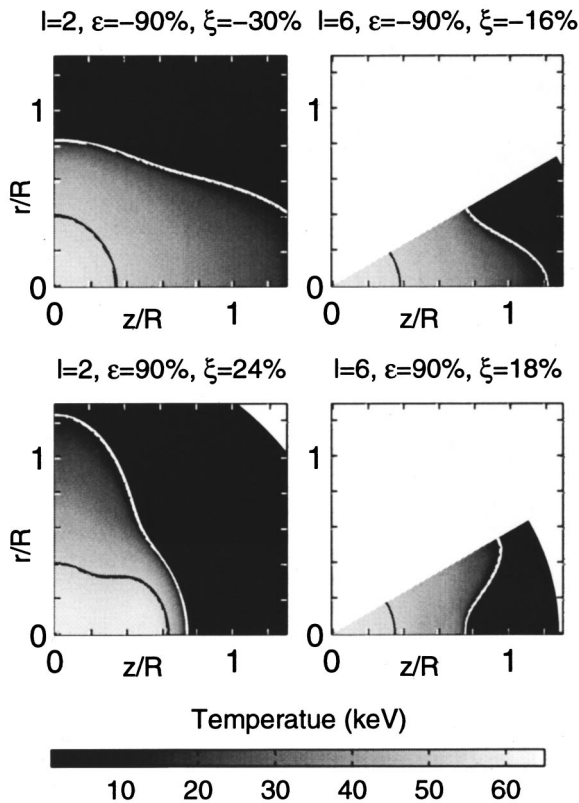


FIG. 11. Temperature contours of a 2D self-similar solution for $l=2$ and 6 with negative and positive amplitudes. The white and black contours correspond to 4 and 50 keV, respectively.

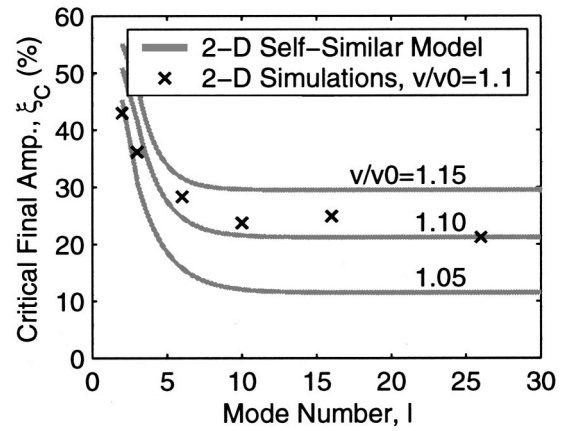


FIG. 12. The critical final amplitude versus the perturbation mode number. The simulation results for targets with an implosion velocity 10% higher than the symmetric ignition velocity ($v/v_0=1.1$) are compared with the self-similar model results for $v/v_0=1.05, 1.1$ and 1.15 .

(bubble) on axis configuration for $\epsilon>0$ ($\epsilon<0$) for both $l=2$ and 6 , high temperature contours are in an opposite configuration for the $l=2$ case. Since the main thermonuclear burn takes place in the high temperature region, we should treat the $l=2$ case with $\epsilon>0$ ($\epsilon<0$) as a bubble (spike) on axis perturbation in contrast to the definition applied to all other mode numbers. Hence, the decrease in the required velocity needed for ignition shown for $l=2$ in Fig. 9 is related to bubble-on-axis configuration and is in agreement with the complete simulations that show that a small bubble-on-axis perturbation can indeed help the ignition of the hot spot.

The physical reason for the apparent anomalous behavior of $l=2$ is that for low enough mode numbers the bubbles become decoupled from the spikes and thus the burn may take place in the bubble alone, which has a higher optical depth than the radius of the unperturbed hot spot.

In Sec. II we analyzed 2D numerical simulations of hot spot implosions and showed (see Fig. 2) that the critical final amplitude, above which the hot spot no longer ignites, decreases monotonically with the perturbation mode number and at high mode numbers it converges asymptotically to the value predicted by Levedahl and Lindl's formula, Eq. (1). While Levedahl and Lindl's model explains only the asymptotic behavior in the high mode number region, the 2D self-similar solutions can be used to explain the entire behavior—from low to high mode numbers. The simulations of Fig. 2 were performed with an implosion velocity 10% higher than the critical implosion velocity needed for the ignition of the symmetric hot spot. Hence, the critical final amplitude for this case can be obtained from the 2D self-similar ignition criteria by intersecting the ignition curves of Fig. 9(b) with the $v/v_0=1.1$ line. In Fig. 12 the self-similar results are compared with the simulation results of Fig. 2. A good agreement between the self-similar model and the simulations is seen. The maximal discrepancy is obtained for mode number $l=2$, for which the self-similar criteria predict a critical amplitude of 50% while in the simulations ignition already fails at amplitudes of 40%.

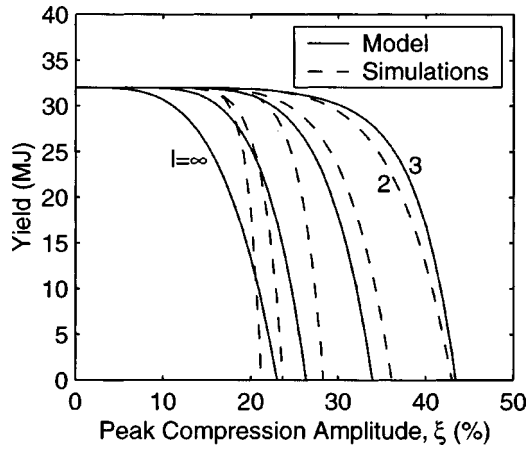


FIG. 13. A comparison between complete 2D simulations and the model [Eq. (6)]. The yield of the perturbed target is shown versus the perturbation amplitude at peak compression for mode numbers $l=2, 3, 6, 10,$ and 26 in the simulations and $3, 4, 6,$ and ∞ in the model (the lines are in sequential order starting from the low modes at the right of the figure).

D. A gain model for a general perturbation

The arguments used to determine the required increase in the implosion velocity needed for ignition can be taken even further in order to give an approximate formula for the yield $Y(v_0, l_0, \xi_0)$ of a general target as a function of the implosion velocity and the perturbation characteristics l_0 and ξ_0 :

$$Y(v_0, l_0, \xi_0) = Y(v_0, \hat{R}_{\text{eff}}(l_0, \xi_0)) \quad (6a)$$

$$= Y(v_0, \hat{R}_{\text{eff}}(l = \infty, \xi = 1 - \hat{R}_{\text{eff}}(l_0, \xi_0))) \quad (6b)$$

$$= Y_{1D}(v_0, \hat{R}_{\text{eff}}(l_0, \xi_0)^{2/5}). \quad (6c)$$

The main assumption in Eq. (6), reflected in the first equality (6a), is that the perturbation affect the gain curve via the reduction of the effective radius of the hot spot and that the relevant effective radius of the hot spot is the same as the effective radius that was defined for the IL. The second equality, (6b), relies on the fact that for high mode numbers only the inner clean radius contribute to ignition, $\hat{R}_{\text{eff}}(l = \infty, \xi) = 1 - \xi$, and translates the imposed perturbation of any l_0 to a short wavelength perturbation with the same effective ignition radius. The last equality, (6c), uses Levedahl and Lindl's formula²³ to connect between the effective short wavelength perturbation and a 1D simulation with reduced implosion velocity.

Equation (6) gives an estimate for the effect of perturbations on the yield of a general target, based only on 1D simulations of the given target with an implosion velocity reduced by $\hat{R}_{\text{eff}}(l, \xi)^{2/5}$, where $\hat{R}_{\text{eff}}(l, \xi)$ is given by the self-similar solutions [Fig. 9(a)]. We tested this formula against our complete 2D simulations results. The comparison is given in Fig. 13, which shows the yield as a function of the perturbation amplitude at peak compression for different perturbation mode numbers. It is seen that the model gives the right behavior and is in good agreement with the simulations compared to what could be *a priori* expected form such a simplified model. Still, it is important to note the two main

differences seen between the model and the simulations. First, the critical amplitudes predicted by the self-similar solutions are slightly higher than the ones obtained by the simulations in the very low mode numbers region $l \leq 3$ (see also Fig. 12), this difference, however, corresponds to a shift of one unit only in the mode numbers ($l=2$ in the simulation correspond to $l=3$ in the model). Second, the shape of the gain curve is sharper in the simulations compared to the model, which is a results of the approximation (6c) which define an effective reduction in the implosion velocity by extending Levedahl and Lindl's formula²³ to regions of gains higher than one.

When a multimode perturbation is imposed, the effective radius, or effective amplitude $\xi_{\text{eff}} = 1 - \hat{R}_{\text{eff}}$, needs to be defined as a function of the spectrum $\xi(l)$ of the perturbation at the time of hot spot stagnation. For each mode l of the perturbation, an effective amplitude $\xi_{\text{eff}}(l, \xi(l))$ would be defined such that the perturbation $[l, \xi(l)]$ would have the same effect as the perturbation $[l = \infty, \xi_{\text{eff}}(l, \xi(l))]$. Then the effective amplitude of the overall multimode perturbation would be

$$\xi_{\text{eff}} = \sqrt{\sum_l \xi_{\text{eff}}^2(l, \xi(l))}. \quad (7)$$

We now need to define the effective amplitudes $\xi_{\text{eff}}(l, \xi(l))$ for each mode number. As was pointed out (see Fig. 9), the effect of a single mode long wavelength perturbation is highly nonlinear with the perturbation amplitude—the effect of small amplitudes on the effective radius is very mild and it becomes prominent only when the amplitude gets large enough. When considering a multimode perturbation one should therefore take into account that while the amplitude of a specific mode might be in the “small amplitude” region, the overall amplitude of the multimode perturbation might be much larger (typically in the 20%–40% region). Thus we need to use the effective physical amplitude of many adjacent modes instead of the individual amplitudes, which are much smaller, thus effectively reducing the resolution in the mode space (in some analogy to Haan's saturation model¹⁸ for Rayleigh–Taylor growth). We propose that an adequate way to account for the combined effect of the modes is to define the effective amplitudes of the given modes as

$$\xi_{\text{eff}}(l, \xi(l)) = \frac{\xi(l)}{\xi_c(l, \hat{v})} \xi_c(l = \infty, \hat{v}), \quad (8)$$

where $\xi_c(l, \hat{v})$ is the critical amplitude as given in Fig. 12 and \hat{v} is the ratio between the actual velocity v_0 of the target and the velocity that causes failure of the hot spot in the symmetric case.

The yield of a multimode perturbation is thus given in our model by Eq. (6), where $R_{\text{eff}} = 1 - \xi_{\text{eff}}$ and ξ_{eff} is given by Eqs. (7) and (8).

We tested our approach on the results of multimode simulations performed by the Laboratory for Laser Energetics (LLE) group for the direct drive ignition capsule of the NIF.⁴² Mckenty, Goncharov *et al.* had shown that the target gain could be well represented in terms of an effective amplitude defined as the route of a weighted sum-in-quadrature of the amplitudes of the different modes at the end of the

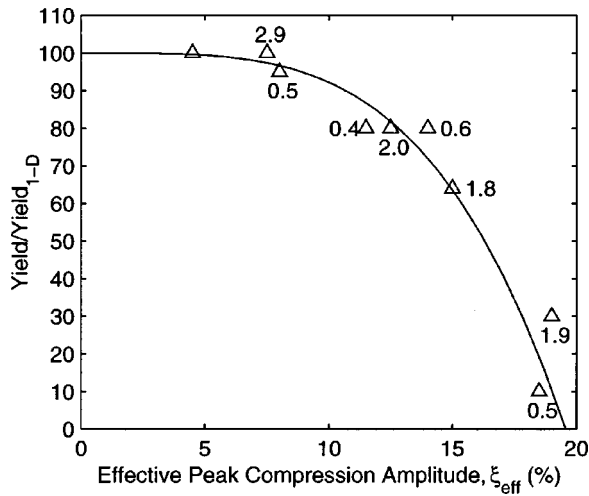


FIG. 14. The yield of a NIF direct drive target subjected to different multi-mode perturbations (Ref. 42) as a function of the effective amplitude of the perturbation at peak compression [Eq. (7) assuming $\hat{v}=1.13$ (Ref. 42)]. Each point is indicated by the ratio between the sum-in-quadrature of the peak compression amplitudes of all modes with $l < 10$ and the corresponding sum for $l > 10$.

acceleration phase.⁴² Their best fit for these weights is 0.06 and 1 for the long ($l < 10$) and short ($l \geq 10$) wavelengths, respectively. This separation to long and short wavelength and the larger effect of the short wavelength perturbations is in accordance with the critical amplitude of the different modes, Fig. 12, which reach a plateau around $l = 10$. The approach presented here, Eq. (8), actually uses these critical amplitudes to define the specific weights of the different modes. Note, however, that our approach is defined for the amplitudes at the time of stagnation rather than for the end of the acceleration phase. Using the spectrum of perturbation amplitudes at the time of stagnation for the same target used in Ref. 42, we have calculated the effective amplitude of a mixed region at stagnation by Eqs. (7) and (8). Figure 14 shows the yield of the target, subjected to different multi-mode perturbations, as a function of the effective amplitude at the time of stagnation. It is seen that the yield indeed depends, to a good approximation, on this effective amplitude alone. Note that the model holds for a wide range of perturbation spectra with a large variability in the relative contribution of low and high perturbation modes.

V. CONCLUSIONS

Ignition conditions for perturbed hot spots were investigated using both full 2D numerical simulations and a model based on new 2D self-similar solutions. Using 2D numerical simulations the critical final hot spot perturbation amplitude (at peak compression), above which the hot spot no longer ignites, was obtained as a function of the perturbation mode number. It was found that at mode numbers larger than about 10 the bubbles evolving from the Rayleigh–Taylor instability no longer contribute to the ignition process and the critical final amplitude of the hot spot perturbation thus no longer depends on the perturbation mode number.

The one dimensional self-similar approach for obtaining the ignition criteria¹⁰ was extended to treat perturbed hot

spots. By letting the hot spot propagate into an outside perturbed density profile that decreases as $\rho_{\text{out}} \propto r^{-1}(1 + A \cos \theta)$, no new dimensional parameters are introduced to the problem and the behavior remains self-similar. The resulting 2D self-similar solutions were used to produce the $\rho R - T$ plane ILs for different final perturbation mode number and amplitude. The ILs obtained are higher than the IL of the symmetric hot spot, reflecting the fact that perturbed hot spots require a larger ρR in order to ignite. The higher the mode number is and the larger is its final amplitudes, the higher is the IL.

The 2D ILs were related to higher implosion velocities needed for the ignition of perturbed hot spots, using the 1D Levedahl–Lindl high mode number limit scaling,²³ which relates the perturbation amplitude in the limit of high mode number with the required increase in implosion velocity needed for ignition. Since for low mode numbers the bubbles still contribute to the ignition process the required increase in the driver energy is lower compared to Levedahl and Lindl's prediction for the limit of high mode number perturbations. These results were compared with the full 2D numerical simulations at low and high mode numbers, and a good agreement was found for the entire region of mode numbers. An interesting result and picture had emerge for mode number $l = 2$: The 2D self-similar approach predicts that a small perturbation may actually help the ignition because the long wavelength makes it possible for the burn to take place in the two bubbles independently with negligible interference from the cold spikes, enabling the ignition and burn to occur at somewhat lower ρR . This prediction of the 2D self-similar ignition criteria had been verified by full 2D simulations, which indeed show a slight increase in the total yield due to small perturbations of mode number $l = 2$.

Using the self-similar ignition lines together with Levedahl and Lindl's scaling, we proposed a model for predicting the gain of a general target with a single mode perturbation based only on 1D simulations with an appropriate decrease in the implosion velocity. The model shows good agreement with full numerical simulations both for high and for low mode numbers. An extension of this single mode gain-perturbation model to the more general case of multi-mode spectra is suggested, by defining an effective mix region thickness which weights each mode according to its single mode gain-perturbation amplitude curve. With this effective final amplitude, the gain of a given target subjected to a given multimode perturbation spectra, is given. Good agreement to results of NIF direct drive full 2D multi-mode simulations is obtained.

ACKNOWLEDGMENTS

We are very thankful to C. P. Verdon, V. N. Goncharov, P. W. McKenty, S. Skupsky, R. L. McCrory, J. D. Lindl, I. Kelson, R. Sari, D. Oron, and Y. Srebro for helpful discussions and important comments. Special thanks to C. P. Verdon for supplying us the profiles of the canonical $\alpha = 3$ direct drive design of NIF^{29–31} and to V. N. Goncharov and P. W. McKenty for sharing with us their results of the multimode simulations before publication.⁴² We also thank LLE for the

hospitality during our visits in the years 1995–1998. Finally, we would like to thank the anonymous referee for providing us the opportunity to explain the mechanism of extension of Levedahl and Lindl's model to gain prediction.

- ¹J. D. Lindl, Phys. Plasmas **2**, 3933 (1995).
- ²S. W. Haan, S. M. Pollaine, J. D. Lindl, L. J. Suter, R. L. Berger, L. V. Powers, W. E. Alley, P. A. Amendt, J. A. Futterman, W. K. Levedahl, M. D. Rosen, D. P. Rowley, R. A. Sacks, A. I. Shestakov, G. L. Strobel, M. Tabak, S. V. Weber, G. B. Zimmerman, W. J. Krauser, D. C. Wilson, S. V. Coggeshall, D. B. Harris, N. M. Hoffman, and B. H. Wilde, Phys. Plasmas **2**, 2480 (1995).
- ³V. B. Rozanov, C. P. Verdon, M. Decroisette, S. Yu. Gus'kov, J. D. Lindl, K. Nishihara, and H. Takabe, in *Energy from Inertial Fusion*, edited by W. J. Hogan (International Atomic Energy Agency, Vienna, 1995), p. 56.
- ⁴See National Technical Information Service Document No. SAND792454 (M. W. Widner, "Fuel energy balance studies of pellet ignition requirements," Sandia National Laboratories, SAND-79-2454). Copies may be ordered from the National Technical Information Service, Springfield, Virginia 22161.
- ⁵R. C. Kirkpatrick, Nucl. Fusion **19**, 69 (1979).
- ⁶S. Atzeni and A. Caruso, Nuovo Cimento B **80**, 71 (1984).
- ⁷J. D. Lindl, *International School of Plasma Physics Piero Caldirola: Inertial Confinement Fusion*, edited by A. Caruso and E. Sindoni (Editrice Compositori, Bologna, Italy, 1988), pp. 617–631.
- ⁸M. M. Basko, Nucl. Fusion **30**, 2443 (1990).
- ⁹O. B. Vygovskii, S. Yu. Gos'kov, D. V. Il'in, A. A. Levkovskii, V. B. Rozanov, and V. E. Sherman, "Criterion of formation of a thermonuclear burn wave in deuterium–tritium targets," translated from a preprint (manuscript) of the Lebedev Physics Institute (Plenum, Moscow, 1993), p. 85.
- ¹⁰R. Kishony, E. Waxman, and D. Shvarts, Phys. Plasmas **4**, 1385 (1997).
- ¹¹V. V. Neudachin and P. V. Sasorov, Sov. J. Plasma Phys. **14**, 567 (1988).
- ¹²V. V. Neudachin and P. V. Sasorov, Nucl. Fusion **33**, 475 (1993).
- ¹³Laboratory for Laser Energetics *LLE Review* 23, 125 NTIS Document No. DOE/DP/40200-05 (1985). Copies may be obtained from the National Technical Information Service, Springfield, VA 22161.
- ¹⁴R. L. McCrory and C. P. Verdon, *International School of Plasma Physics Piero Caldirola: Inertial Confinement Fusion (1988)*, edited by A. Caruso and E. Sindoni (Editrice Compositori, Bologna, Italy, 1988), p. 83.
- ¹⁵S. Atzeni, Europhys. Lett. **11**, 639 (1990).
- ¹⁶S. Atzeni, Laser Part. Beams **9**, 223 (1991).
- ¹⁷S. Atzeni, Part. Accel. **37–38**, 495 (1992).
- ¹⁸S. W. Haan, Phys. Rev. A **39**, 5812 (1989).
- ¹⁹W. J. Krauser, N. M. Hoffman, D. C. Wilson *et al.*, Phys. Plasmas **3**, 2084 (1996).
- ²⁰M. M. Marinak, Phys. Plasmas **3**, 2070 (1996).
- ²¹D. C. Wilson, P. A. Bradley, N. M. Hoffman *et al.*, Phys. Plasmas **5**, 1953 (1998).
- ²²M. M. Marinak, S. W. Haan, T. R. Dittrich, R. E. Tipton, and G. B. Zimmerman, Phys. Plasmas **5**, 1125 (1998).
- ²³W. K. Levedahl and J. D. Lindl, Nucl. Fusion **37**, 165 (1997).
- ²⁴H. Sakagami and K. Nishihara, Phys. Rev. Lett. **65**, 432 (1990).
- ²⁵R. P. J. Town and A. R. Bell, Phys. Rev. Lett. **67**, 1863 (1991).
- ²⁶J. Hecht, D. Ofer, U. Alon, D. Shvarts, S. A. Orszag, and R. L. McCrory, Laser Part. Beams **13**, 423 (1995).
- ²⁷The nominal gain in our calculations is 20 compared to 35 in C. Verdon's canonical design.
- ²⁸Laboratory for Laser Energetics *LLE Review* 79, 121 NTIS Document No. DOE/SF/19460-317 (1999). Copies may be obtained from the National Technical Information Service, Springfield, VA 22161.
- ²⁹S. V. Weber, S. G. Glendinning, D. H. Kalantar, M. H. Key, B. A. Remington, J. E. Rothenberg, E. Wolfrum, C. P. Verdon, and J. P. Knauer, Phys. Plasmas **4**, 1978 (1997).
- ³⁰S. E. Bodner, D. G. Colombant, J. H. Gardner, R. H. Lehmberg, S. P. Obenschain, L. Phillips, A. J. Schmitt, J. D. Sethian, R. L. McCrory, W. Seka, C. P. Verdon, J. P. Knauer, B. B. Afeyan, and H. T. Powell, Phys. Plasmas **5**, 1901 (1998).
- ³¹C. P. Verdon, private communication (1994).
- ³²D. Ofer, U. Alon, D. Shvarts, R. L. McCrory, and C. P. Verdon, Phys. Plasmas **3**, 3073 (1996).
- ³³D. Ofer, "Nonlinear evolution of the multi mode Rayleigh–Taylor hydrodynamic instability," Ph.D. thesis submitted to the scientific council of the Weizmann Institute of Science, June 1995.
- ³⁴M. M. Basko and J. Johner, Nucl. Fusion **38**, 1779 (1998).
- ³⁵M. C. Herrmann, M. Tabak, and J. D. Lindl, Nucl. Fusion **41**, 99 (2001).
- ³⁶M. C. Herrmann, M. Tabak, and J. D. Lindl, Phys. Plasmas **8**, 2296 (2001).
- ³⁷We would like to thank the anonymous referee for raising this important question.
- ³⁸R. Kishony and D. Shvarts, "Ignition conditions for perturbed hot spots in inertial confinement fusion," Proceedings in print (IAEA TECDOC, Vienna, 2001).
- ³⁹The effective ρR is defined in Eq. (5) below and is determined by the parameter s .
- ⁴⁰The amplitude ξ depends on a definition of the boundary of the hot spot. We chose to define the hot spot by the contour of a temperature of 4 keV.
- ⁴¹As was explained earlier, we are limited to values of ξ that are lower than the specific value that is obtained for $\epsilon \rightarrow 1$.
- ⁴²P. W. McKenty, V. N. Goncharov, R. P. J. Town, S. Skupsky, R. Betti, and R. L. McCrory, Phys. Plasmas **8**, 2315 (2001).